Hindawi
Mathematical Problems in Engineering
Volume 2020, Article ID 2653517, 7 pages
https://doi.org/10.1155/2020/2653517

Research Article

Profile Design Method of Twin-Screw Compressor Rotors Based on the Pixel Solution

Zhihuang Shen

College of Mechanical and Energy Engineering, Jimei University, Xiamen 361021, China

Correspondence should be addressed to Zhihuang Shen; shenzhihuang2008@sina.com

Received 25 March 2020; Revised 16 July 2020; Accepted 24 August 2020; Published 25 September 2020

Academic Editor: Salvatore Strano

A new design method based on pixel solution is proposed to achieve an efficient and high-precision design of a twin-screw rotor profile. This method avoids the complex analytic calculations in the traditional envelope principle. The best approximation of the pixels of the rotor conjugate motion sweeping surface in the lattice screen pixels is illuminated using a specific color. The sweeping surface of the screw rotor single-tooth profile is roughly scanned to capture the base point set of the sweeping surface boundary pixels. The chord length and tilt angle of each interval are calculated using the value of the base point set to adjust the position, phase, and magnification of each interval sweeping surface. Each interval sweeping surface is finely scanned to capture the data point set of the subinterval, and then the data point set is converted to the same coordinate system to generate the conjugated rotor profile. Finally, an example is used to verify the feasibility and adaptability of this method. The approach provided can be used to design screw rotor profiles with high precision.

1. Introduction

Twin-screw compressors have the advantages of reliable operation, long service life, compact structure, and high energy efficiency and are, thus, widely used in automotive, compression, and refrigeration, among other industrial fields. A pair of meshing screw rotors forms the key component of the twin-screw compressor, and the rotor profile is the main factor determining the performance of the compressor. Therefore, the methodology used to design a precision screw rotor profile efficiently is particularly important. With the improvements in the technological level and calculation conditions, many representative rotor profiles and their design methods have been developed in recent years.

Litvin and Fuentes [1] derived an analytical calculation process of the forming tool profile for machining gears, which could also be used to design screw rotors. Xing et al. [2, 3] designed a rotor profile based on screw rotor geometry, thermal characteristics, and the contact condition between the male rotor and the female rotor, establishing the rotor and the grinding wheel. Stosic et al. [4, 5] used the conjugate principle to design the *N* profile. Spitas proposed a method to discretize the gear tooth surface into several involutes to calculate the conjugate tooth profile [6]. For the above-mentioned literature, the mathematical model of the analytic gearing envelope method was accurate enough. However, it was identified that they have a computing problem concerning the complex contact line equation. Owing to the complexity of the equation of the contact line, the computing process of the equation led to the formation of a singular point and an uneven distribution of the generated profile data.

Many scholars have, thus, been continuously working toward finding an easier and more comprehensive method to substitute the analytic gearing envelope method. The point vector envelope method was proposed to calculate the forming tool profile of the spiral surface by He et al. [7]. Lyashkov and Panchuk [8] used the CAD technology to calculate the tool profile of the screw pump. Yang et al. [9] used MATLAB and Unigraphics motion simulation to build the 3D model of the screw rotor and then used edge detection of the graphics method and the shape algorithm to calculate the tool profile. Wu et al. [10] proposed a radial-ray

shooting method to simulate the form grinding process of a threaded cylindrical workpiece, such as a spur, helical gear, and screw. The profile of the workpiece can precisely be determined from the intersecting points on each ray without solving the simultaneous system equations of locus and the equation of meshing. However, Wu omitted the details of the calculation of the intersecting points.

To generate the conjugate rotor profile, a new method of designing a screw rotor profile, based on pixel solution, has been proposed in this study. This method requires multiple adjustments of the pose and the magnification of the conjugate motion sweeping surface by the known rotor. The critical pixels in the screen pixel matrix of the subinterval sweeping surface were captured to rebuild the unknown rotor profile. The pixel solution method generates a grinding profile without establishing and computing the contact line equation. The improved pixel solution has an automatic scanning position adjustment function and solves the problem of uneven local data points caused by the single scanning direction in the digital graphic scanning method and pixel solution proposed by the studies mentioned earlier [11, 12]. Finally, an example has been proposed to show the difference between the pixel solution and the analytic gearing envelope method. The results show that the pixel solution avoids the singular point and uneven distribution of profile data seen in the analytic gearing envelope method. The deviation between the two methods was found to be within -0.002 mm to 0.002 mm.

2. Calculation of the Sweeping Surface

2.1. Coordinate Transformation between Male and Female Rotor. The coordinate system is established to describe the conjugate envelope process of the screw rotors through mathematical equations, as shown in Figure 1. The coordinate systems $O_1x_1y_1$ and $O_2x_2y_2$ are attached to the male and female rotors. a is defined as the distance between the male and female rotors. Parameters r_1 and r_2, φ_1 and φ_2, and w_1 and w_2 are the pitch circle radii, phase angle, and angular velocity of the male and female rotors, respectively. According to the spatial geometric relationship, the coordinate transformation formula between the male and the female rotors is given by

$$M_1 = \begin{bmatrix} -\cos(\varphi_1+\varphi_2) & -\sin(\varphi_1+\varphi_2) & a\cos\varphi_1 \\ -\sin(\varphi_1+\varphi_2) & \cos(\varphi_1+\varphi_2) & a\sin\varphi_1 \\ 0 & 0 & 1 \end{bmatrix},$$
$$M_2 = \begin{bmatrix} -\cos(\varphi_1+\varphi_2) & -\sin(\varphi_1+\varphi_2) & a\cos\varphi_2 \\ -\sin(\varphi_1+\varphi_2) & \cos(\varphi_1+\varphi_2) & a\sin\varphi_2 \\ 0 & 0 & 1 \end{bmatrix}. \quad (1)$$

2.2. Conjugate Envelope Motion of Rotors. As shown in Figure 2, assuming the female rotor profile coordinates (x_2, y_2) are known, we calculate the profile coordinates (x_1, y_1) of the conjugate male rotor. Both rotors are given a rotational angular velocity of $-w_1$ that enables the male rotor

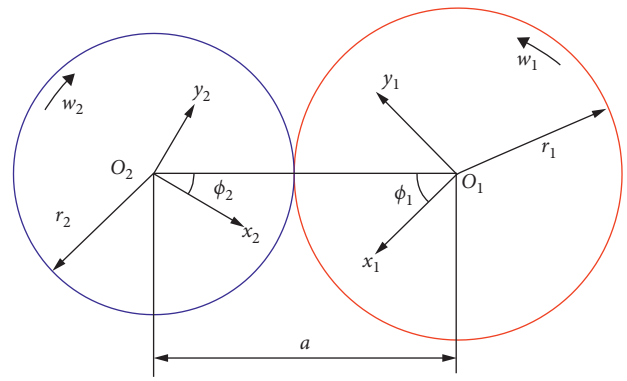

Figure 1: Coordinate relationship of male and female rotors.

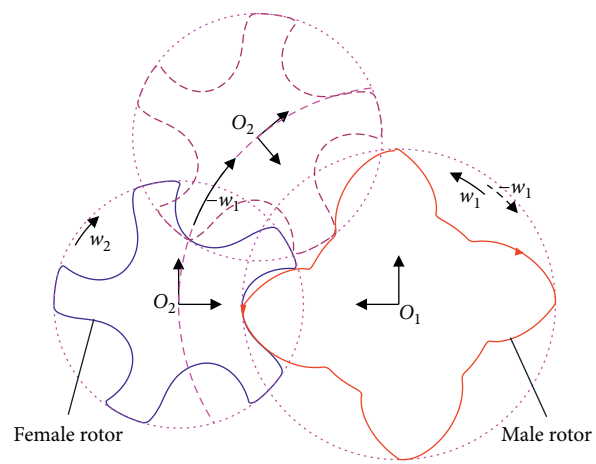

Figure 2: Planetary motion of the female rotor.

to orbit first, after which the female rotor will take planetary motion, while the male rotor stands still. The rotation and revolution angular velocity of the female rotor is w_2 and w_1. The planetary motion of the female rotor envelops the profile of the male rotor. The conjugate envelope process is shown in Figure 3.

3. Principle of Bresenham Algorithm

The line, circle, and ellipse are the basic elements in graphic design. Pixel function is necessary to build the graphics according to the display principle of the monitor and realistic graphic technology. The existing monitor represents a line, approximately, by capturing the nearest pixel point set of the region boundary, rather than by drawing the line from one pixel to another directly. The graph scan conversion illuminates the pixels that are closer to the ideal graph compared with all other pixels in the matrix of the screen in a specified color. For instance, in Figure 4, the black line can only be approximated by lightening the blue pixels which are nearest to the blue line. The Bresenham algorithm is adopted for the line scan conversion due to its high efficiency in drawing lines. In the Bresenham algorithm, the active pixel moves one unit with every frequency change along the principal direction. The secondary directional movement is determined by the midpoint deviation discrimination [13, 14].

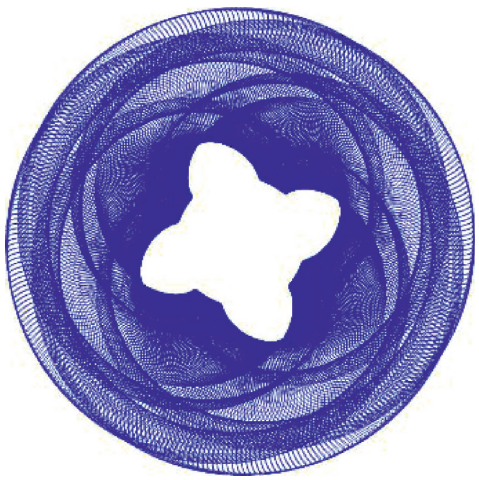

Figure 3: Male rotor enveloped by the female rotor.

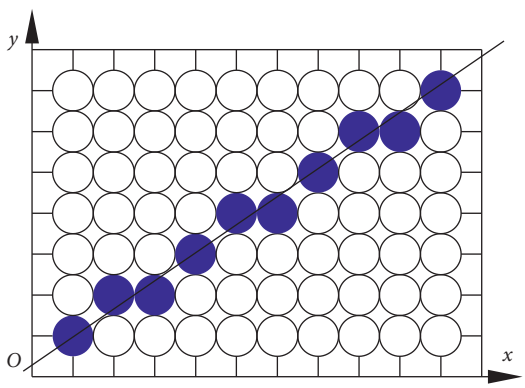

Figure 4: Line scan conversion.

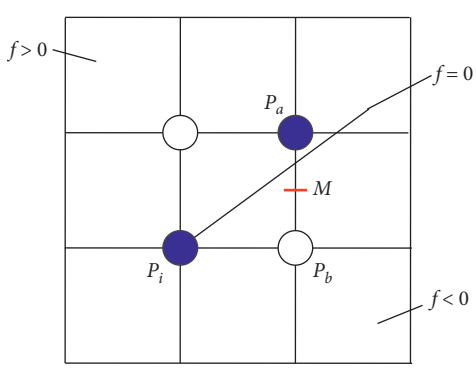

Figure 5: Midpoint Bresenham algorithm.

The starting point of the ideal line is defined as $P_0(x_0, y_0)$, and the ending point is defined as $P_n(x_n, y_n)$. The implicit function equation of the line is described as

$$f(x, y) = y - ux - v = 0, \tag{2}$$

where u is the linear slope and v is the intercept in the y direction. As shown in Figure 5, assuming that the active pixel coordinate point is $P_i(x_i, y_i)$ and by moving one unit along the x direction, the next pixel can be chosen between $P_a(x_i + 1, y_i + 1)$ and $P_b(x_i + 1, y_i)$. The midpoint of P_a and P_b is $M(x_i + 1, y_i + 0.5)$. P_a is chosen when the ideal line is above the midpoint M, indicating that P_a is nearer to the line compared to P_b, as if otherwise, P_b would have been chosen.

Midpoint deviation discrimination is integrant to acquire the next pixel after the first step. The midpoint M, in the implicit function equation, is substituted to build the midpoint deviation discrimination d_i and is given by

$$d_i = f(x_i + 1, y_i + 0.5) = y_i + 0.5 - u(x_i + 1) - v. \tag{3}$$

P_a is chosen when $d_i < 0$ and the ideal line is above the midpoint M, which means that the active pixel moves one unit along the y direction. P_b is chosen when $d_i > 0$ and the ideal line is below the midpoint M, which means that the active pixel has no movement. Either P_a or P_b can be chosen when $d_i = 0$, indicating that M is located on the line. The deviation discrimination can also be presented as [15]

$$y_{i+1} = \begin{cases} y_i + 1, & d_i < 0, \\ y_i, & d_i \geq 0. \end{cases} \tag{4}$$

Recurrence formulation is a prerequisite when the midpoint deviation discrimination d_i is acquired to judge every point on the line continuously. As shown in Figure 6, there are two possibilities when choosing a midpoint to substitute the midpoint deviation discrimination and when choosing the pixel after the active pixel has already moved along the principle direction.

The midpoint coordinates of the next step are $M'(x_i + 2, y_i + 1.5)$. When $d_i < 0$, the midpoint deviation discrimination can be prescribed as

$$\begin{aligned} d_{i+1} &= f(x_i + 2, y_i + 1.5) = y_i + 1.5 - u(x_i + 2) - v \\ &= y_i + 0.5 - u(x_i + 1) - v + 1 - u = d_i + 1 - u. \end{aligned} \tag{5}$$

The midpoint coordinate of the next step is $M'(x_i + 2, y_i + 0.5)$. When $d_i \geq 0$, the midpoint deviation discrimination can be prescribed as

$$\begin{aligned} d_{i+1} &= f(x_i + 2, y_i + 0.5) = y_i + 0.5 - u(x_i + 2) - v \\ &= y_i + 0.5 - u(x_i + 1) - v - u = d_i - u. \end{aligned} \tag{6}$$

4. Principle of Pixel Solution

The pixel solution first illuminates the best approximation pixels of the rotor conjugate swept surface in the screen pixel lattice with the specified color and then adjusts the pose and magnification of the sweeping surface. The conjugate rotor profile is calculated by capturing the coordinates of the best approximation pixel. The best approximation pixel is the boundary pixel that distinguishes between the specified color and the background color of the screen. The calculation procedure is divided into the following steps:

(1) Assuming the female rotor profile is known, the trajectory of its planetary motion is obtained by the envelope principle, as shown in Figure 7.

(2) The sweeping surface of the female rotor profile is adjusted and enlarged (magnification is K) to fill the monitor screen (display resolution of the monitor is

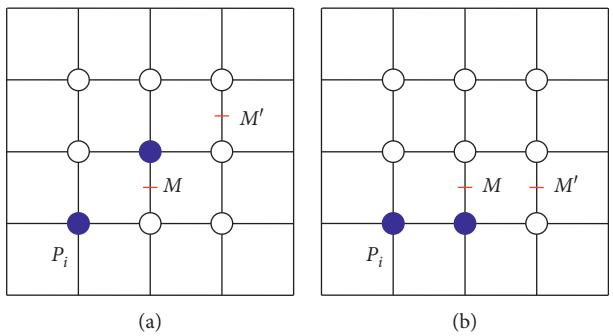

Figure 6: Recurrence formulation of midpoint deviation discrimination. (a) $d_i < 0$ and (b) $d_i \geq 0$.

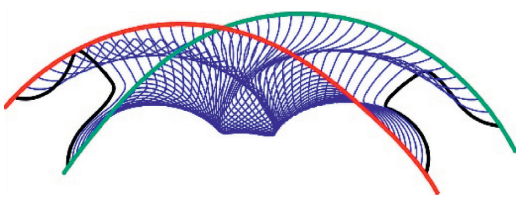

Figure 7: Planetary trajectory of the female rotor profile.

$x_s \times y_s$). According to the Bresenham algorithm, blue color (RGB = (0, 0, 255)) was used to lighten the best approximated pixels of the enveloping surface in the pixel matrix of the screen and the other region was lightened by yellow color (RGB = (255, 255, 0)), as shown in Figure 8.

(3) The sweeping surface is rough, scanning to get the basic point sets of the conjugate rotor profile. The basic point sets are $P_0, P_1, P_2, \ldots, P_i, \ldots, P_m$, where m is the number of the segmented intervals of the sweeping surface (in the actual calculation, $m = 200$).

(4) The sweeping surface is divided into several basic intervals, and A is the i-th interval. As shown in Figure 9, the chord length s_i and the chord length tilt angle α_i of the sweeping surface in the interval A can be calculated according to the coordinate of the points P_i and P_{i+1}.

(5) The chord length s_i and chord length tilt angle α_i are used to adjust the position, phase, and magnification of the sweep surface between the two points P_i and P_{i+1}. The purpose of the readjustment is to ensure the A interval fills the entire screen smoothly, as shown in Figure 10. The coordinate system changed from S_0 to S_i during the readjustment; the rotation angle and the new magnification are α_i and $K_i = (x_s/s_i)K$, respectively. The critical pixels of the interval A are captured, and the critical pixel set is $P_{i,0}, P_{i,1}, \ldots, P_{i,t_i}, \ldots, P_{i,n_i}$. The critical pixel sets of the other intervals can be obtained using the abovementioned method, as shown in Table 1.

(6) After capturing the critical pixel sets of each interval, they need to be transformed into the unified coordinate system. As shown in Figure 11, OXY is the unified coordinate system, $x_s \times y_s$ is the screen resolution, and $O_i x_i y_i$ is the coordinate of each interval. The formula for transforming critical pixel sets of each interval to the unified coordinate system is given by

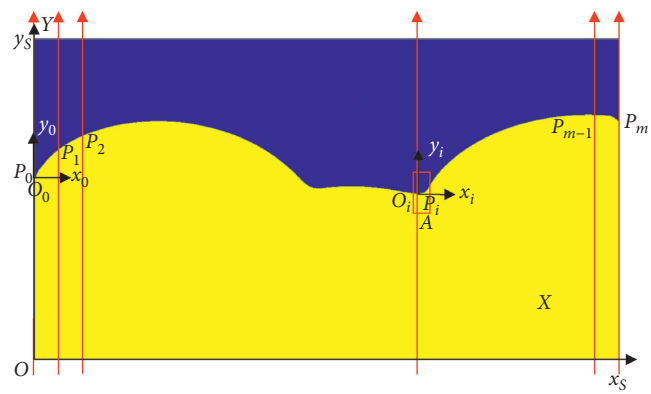

Figure 8: Sweeping surface posture adjustment and basic point set scanning.

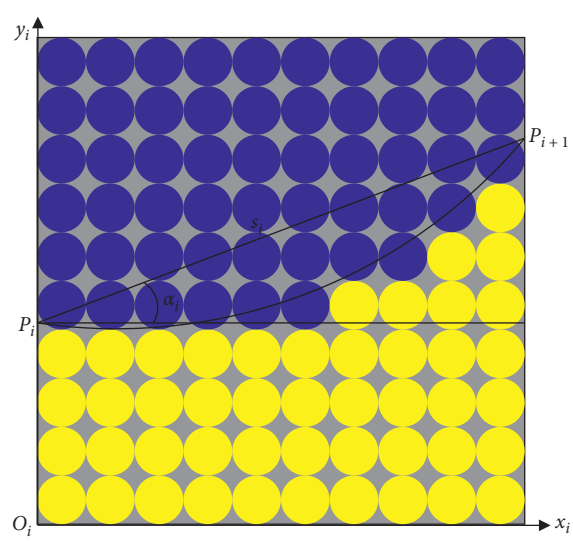

Figure 9: Local enlargement diagram of interval A.

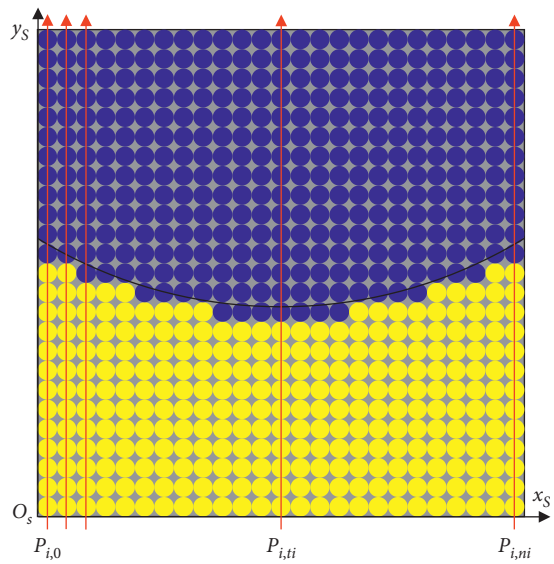

Figure 10: Regeneration of sweeping surface of interval A.

Table 1: Critical pixel sets of each interval.

Interval	0	1	...	t	...	n
0	$P_{0,0}$	$P_{0,1}$	...	P_{0,t_0}	...	P_{0,n_0}
1	$P_{1,0}$	$P_{1,1}$	...	P_{1,t_1}	...	P_{1,n_1}
...	...	...	...	...	...	...
i	$P_{i,0}$	$P_{i,1}$	...	P_{i,t_i}	...	P_{i,n_i}
...	...	...	...	...	...	...
m	$P_{m,0}$	$P_{m,1}$	...	P_{m,t_m}	...	P_{m,n_m}

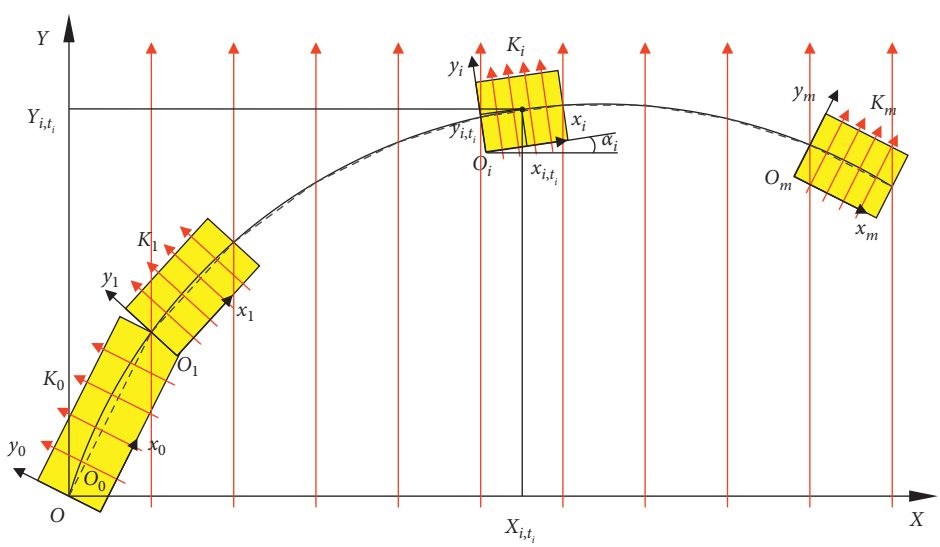

Figure 11: Coordinate transformation of each interval.

$$\begin{bmatrix} X_{i,t_i} \\ Y_{i,t_i} \end{bmatrix} = \frac{1}{K_i} \begin{bmatrix} \cos\alpha_i & -\sin\alpha_i \\ \sin\alpha_i & \cos\alpha_i \end{bmatrix} \begin{bmatrix} x_{i,t_i} + X_{i,0} \\ y_{i,t_i} + Y_{i,0} \end{bmatrix}, \quad (7)$$

where $(X_{i,0}, Y_{i,0})$ is the coordinate of $P_{i,0}$.

(7) As shown in Figure 12, through the above method, tens of thousands of sweeping surface profile points can be captured. The profile points can be reorganized by setting an offset to meet the accuracy requirement of the male rotor, as shown in Figure 13.

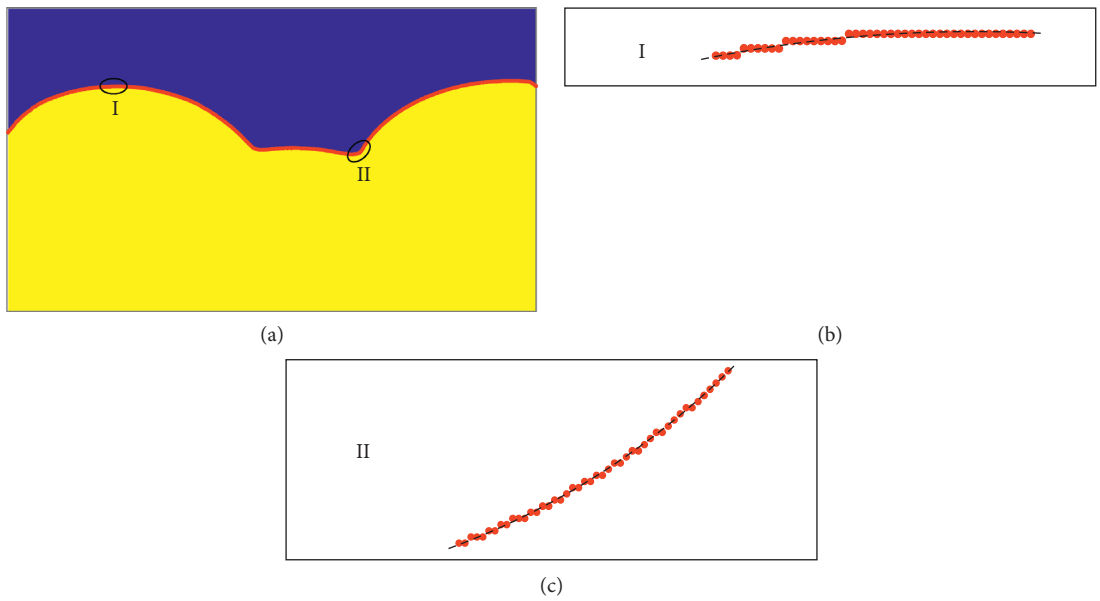

Figure 12: Profile data of sweeping surface. (a) Profile of sweeping surface. (b) Enlarged profile of area I. (c) Enlarged profile of area II.

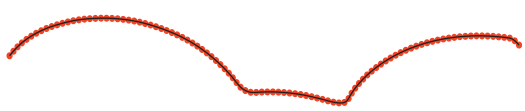

Figure 13: Restructured male rotor profile.

5. Numerical Examples

An example of the rotors from a screw compressor manufacturer was investigated to verify the correctness and the feasibility of the method proposed; the parameters of the rotors are as given in Table 2. Assuming that the female rotor profile is known, the profile of the male rotor needs to be calculated. Figure 14 shows the cross-sectional contour of the female rotor. The selected screen resolution was 1440×900.

The analytic gearing envelope method and the pixel solution are adopted to calculate the male rotor profile. When using the pixel solution, the chosen computer screen has a resolution of 1440×900 and the magnification of the male rotor was $K_1 = 50$. After performing the above steps, 38,152 points of the male rotor were collected. The male rotor profile developed using different generating methods was compared. The result is shown in Figures 15 and 16.

It can be seen from Figure 15 that the performance of the pixel solution was clearly better than the analytic gearing envelope method and that there are no singular points or appearance of uneven distribution phenomena. Figure 16 showed that the deviation between different male rotor profiles, generated using the pixel solution and the analytic gearing envelope methods, was within −0.002 mm to 0.002 mm.

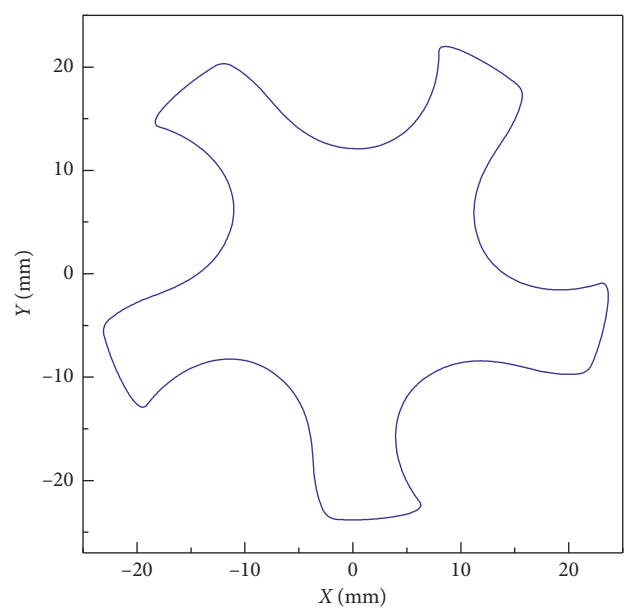

Figure 14: Profile of female rotors.

Table 2: Parameters of the rotors.

Type	Male	Female
Revolving direction	Right hand	Left hand
Number of teeth	5	4
Outer diameter (mm)	47.621	59.795
Root diameter (mm)	24.209	36.380
Lead (mm)	145	116
Helical angle (deg)	45.316	
Center distance (mm)	42	

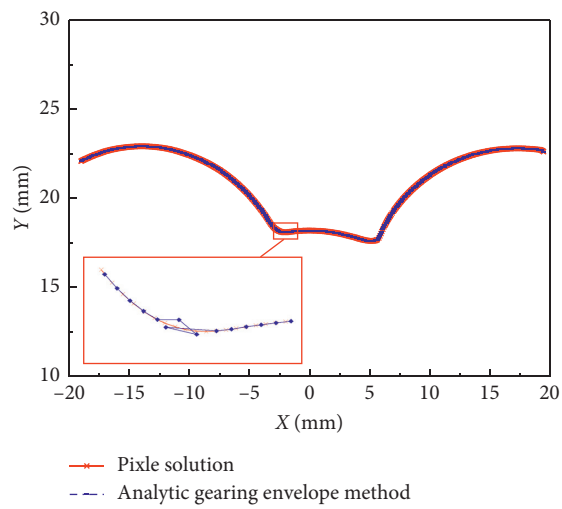

Figure 15: Comparison of the male rotor profile.

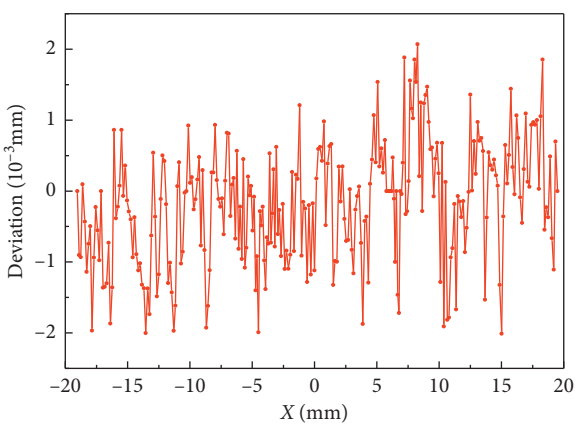

Figure 16: Normal deviation of the male rotor profile.

6. Conclusions

This study presents a pixel solution method, based on computer scanning graphics to generate a conjugate rotor profile, that avoids the difficulties that appear in the analytical gearing envelope method, by using the complex nonlinear equations of the contact line. Conjugate rotor profiles were collected by scanning the pixel matrix of the screen and capturing the coordinates of the indicated color of the best possible pixels, guaranteeing the accuracy of the generated profile.

As shown by the numerical examples, the deviation between the different conjugate rotor profiles, generated by the pixel solution and the analytic gearing envelope method, was within −0.002 mm to 0.002 mm. The results showed that pixel solution is a powerful tool to generate the conjugate rotor profile of the rotors and that it is also suitable for threaded cylindrical workpieces, such as helical gears, worms, spurs, and millings, among others.

Data Availability

The profile data and normal deviation of the male rotor used to support the findings of this study are available from the corresponding author upon request.

Conflicts of Interest

The authors declare that they have no conflicts of interest.

Acknowledgments

This work was financially supported by the Science and Technology Project of Fujian Province, China (project no. 2018J05087), and the Science and Technology Department Project of Fujian (project no. JK2017025).

References

[1] F. L. Litvin and A. Fuentes, *Gear Geometry and Applied theory*, Cambridge University Press, Cambridge, UK, 2004.

[2] Z. Xing, *Screw Compressors: Theory, Design and Application,* Machine Press, Beijing, China, 2000, in Chinese.

[3] J. Lu, Y. Tian, and Z. Xing, "Calculation of conjugated rotor profiles generation for twin-screw compressors based on discrete data," *Compressor Technology*, vol. 275, no. 3, pp. 1–5, 2019, in Chinese.

[4] N. Stosic, I. K. Smith, A. Kovacevic, and E. Mujic, "Geometry of screw compressor rotors and their tools," *Journal of Zhejiang University-Science A*, vol. 12, no. 4, pp. 310–326, 2011.

[5] N. Stosic, I. Smith, and A. Kovacevic, *Screw Compressors: Mathematical Modelling and Performance calculation*, Springer Science & Business Media, Berlin, Germany, 2005.

[6] V. Spitas, T. Costopoulos, and C. Spitas, "Fast modeling of conjugate gear tooth profiles using discrete presentation by involute segments," *Mechanism and Machine Theory*, vol. 42, no. 6, pp. 751–762, 2007.

[7] K. He, G. Li, Y. Du, and Y. Tang, "A digital method for calculation the forming cutter profile in machining helical surface," *International Journal of Mechanical Sciences*, vol. 155, pp. 370–380, 2019.

[8] A. A. Lyashkov and K. L. Panchuk, "Computer modeling of a pump screw and disc tool cross shaping process," *Procedia Engineering*, vol. 113, pp. 174–180, 2015.

[9] J. Yang, F.-H. Sun, and Z. Lu, "Solving the screw compressor rotor-forming grinding wheel using the edge detection method based on the graphic method," *Proceedings of the Institution of Mechanical Engineers, Part E: Journal of Process Mechanical Engineering*, vol. 233, no. 5, pp. 967–979, 2019.

[10] Y.-R. Wu, Z.-H. Fong, and Z.-X. Zhang, "Simulation of a cylindrical form grinding process by the radial-ray shooting (RRS) method," *Mechanism and Machine Theory*, vol. 45, no. 2, pp. 261–272, 2010.

[11] Z. Shen, B. Yao, W. Teng, W. Feng, and W. Sun, "Generating grinding profile between screw rotor and forming tool by digital graphic scanning (DGS) method," *International Journal of Precision Engineering and Manufacturing*, vol. 17, no. 1, pp. 35–41, 2016.

[12] Z. Shen, J. Liu, P. I. Jun et al., "A method of calculating forming wheel profile for grinding involute worm based on pixel solution," *Journal of Xiamen University (Natural Science)*, vol. 57, no. 5, pp. 736–740, 2018, in Chinese.

[13] A. Hashemian and S. F. Hosseini, "An integrated fitting and fairing approach for object reconstruction using smooth NURBS curves and surfaces," *Computers & Mathematics with Applications*, vol. 76, no. 7, pp. 1555–1575, 2018.

[14] Z. Duan, N. Wang, J. Fu, W. Zhao, B. Duan, and J. Zhao, "High precision edge detection algorithm for mechanical parts," *Measurement Science Review*, vol. 18, no. 2, pp. 65–71, 2018.

[15] L. Kong, *Basics Tutorial of Computer Graphics,* Tsinghua University Press, Beijing, China, 2008, in Chinese.